Target detection in shallow-water reverberation based on parameter-induced stochastic resonance

2008 J. Phys. A: Math. Theor. 41 105003

(http://iopscience.iop.org/1751-8121/41/10/105003)

IOP PUBLISHING JOURNAL OF PHYSICS A: MATHEMATICAL AND THEORETICAL

J. Phys. A: Math. Theor. **41** (2008) 105003 (13pp) doi:10.1088/1751-8113/41/10/105003

Target detection in shallow-water reverberation based on parameter-induced stochastic resonance

Huiquan Zhang[1], Bohou Xu[1], Zhong-Ping Jiang[2] and Xingxing Wu[2]

[1] Department of Mechanics, State Key Laboratory of Fluid Power Transmission and Control, Zhejiang University, Hangzhou 310027, People's Republic of China
[2] Department of Electrical and Computer Engineering, Polytechnic University, Brooklyn, NY 11201, USA

E-mail: xubohou@zju.edu.cn

Received 2 November 2007, in final form 26 January 2008
Published 26 February 2008
Online at stacks.iop.org/JPhysA/41/105003

Abstract

A method based on parameter-induced stochastic resonance (PSR) is proposed for the target echo detection in the presence of shallow-water reverberation. The signals received by the horizontal sensor array are first preprocessed to form the input to a bistable stochastic resonance (SR) system. The detection decision is then made by a linear correlation detector based on the output of this SR system. The performance of our proposed detection system, in terms of deflections, is derived based on the solutions to the corresponding Fokker–Planck equations (FPE). Using PSR-based techniques, the detection performance can be optimized by tuning the system parameters properly. In addition, numerical simulations are carried out to demonstrate the efficiency and detection performance of our proposed detection system with receiver operating characteristic (ROC) curves, and the results show that it has good performance under the condition of the weak signal-to-reverberation-noise ratio (SRR).

PACS numbers: 05.40.−a, 02.50.−r

1. Introduction

The target detection with active sonar is often limited by the presence of reverberation. It has been an interesting and active research task to improve the detection performance in the presence of shallow-water reverberation, which has been studied for a long time in the acoustic signal processing area. In shallow water, reverberation mostly arises from the sea bottom backscattering caused by the roughness of the sea bottom [1]. According to the point-scattering model [2–4], reverberation can be treated as a random process constructed by a linear superposition of individual echoes emanating from a large number of point reflectors

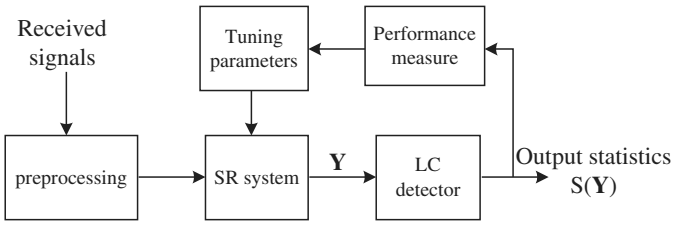

Figure 1. Block scheme for detection.

distributed independently on the sea floor. Therefore, the signal-to-reverberation-noise ratio (SRR) is often very weak. In addition, the reverberation noise is strongly correlated with the transmitted signals. All these make it difficult to detect target echoes in the presence of reverberation.

Since proposed by Benzi *et al* in 1981 to explain the periodicity of ice ages [5–7], stochastic resonance (SR) has been an attractive research area and has been widely applied into a variety of different fields. The counter-intuitive stochastic resonance phenomenon is caused by the cooperation between the stochastic excited nonlinear system and the external deterministic force. Under certain conditions, noise can play an active role in the improvement of system performance. The traditional SR is realized by inserting an optimal amount of additional noise into the SR system to maximize the chosen performance measure, such as the output signal-to-noise ratio (SNR) [8–13]. Recently, a new approach called parameter-induced stochastic resonance was proposed by Xu *et al* to realize the stochastic resonance phenomenon by tuning system parameters without adding noise [14–17]. In signal detection theory, SR also plays a very important role in improving the signal detectability. In [18], it has been shown that the performance of detecting weak sinusoid signals can be improved via SR effect. For some suboptimal detectors, such as sign detector, their performance can be enhanced by adding some noise [19, 20]. In [21–23], techniques based on parameter-induced stochastic resonance (PSR) are applied to binary signal processing and detection. Compared with matched filters, PSR-based approaches have the advantage of being more robust [24, 25].

In this paper, we investigate the applications of PSR techniques to the target echo detection in the presence of shallow-water reverberation. The detection scheme is shown in figure 1. The signals received by the horizontal sensor array are preprocessed in order to extract the echoes from environmental noise. In addition, the spatial frequency of the target echoes is reduced to satisfy the sampling requirement. The preprocessed signals are then processed by the bistable SR system before being sent to the linear correlation (LC) detector. In order to overcome the problem caused by the fixed array length, an unfolding method is suggested to form longer input signals in this detection system. The detection performance is affected by the choice of the SR system parameter values, and thus can be optimized by tuning system parameters properly. Through this research, we attempt to seek a way for applications of PSR techniques to acoustic signal processing.

The rest of this paper is organized as follows. In section 2, the signal and noise models are presented. In addition, the reasons and methods to preprocess the signals received by the horizontal sensor array are introduced. In section 3, a linear correlation detector and the approach to apply PSR techniques are proposed. The numerical simulations are carried out in section 4 to verify the efficiency of our proposed detection system with the receiver operating characteristic curves. Finally, conclusions are presented in section 5.

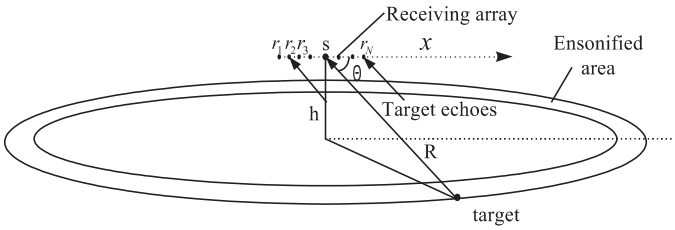

Figure 2. Schematic model of target detection in shallow water.

2. Signal models and preprocessing

Assume that an active sonar emits a pure-tone pulse signal using a non-directive source with frequency f_0 (Hz) and duration T (s). There is a target body on the bottom at the range $R \gg h$ as shown in figure 2, where h is the depth of the sea. Here we assume that the specular reflection of sea bottom is weak, so that normal-mode propagation is negligible. The target echo which is a replica of the transmitted signal arrives at the horizontal array with the angle θ. Thus, assuming that the time when the echo arrives at the first sensor is zero and there is no phase shift, the spacetime target echo signal along the array is expressed as

$$s_{\text{target}}(x,t) = A\cos\left(2\pi f_0 t + \frac{2\pi f_0 \cos\theta}{c}x\right), \qquad -\frac{x\cos\theta}{c} \leqslant t < T - \frac{x\cos\theta}{c}, \tag{1}$$

where A is the amplitude of the echo, c is the acoustic velocity and x is the coordinate of the receiving sensor along the array. The receiving array, with a length of L, consists of sensors disposed at positions $r_1, r_2, r_3, \ldots, r_N$, and the coordinate of r_1 is taken as zero.

According to the point-scattering model [2], the interfering reverberation $R(x,t)$ can be treated as a sum of echoes scattered by the scatterers distributed at the ensonified cirque on the sea bottom, as shown in figure 2. As the number of scatters is large enough, the reverberation can be approximated to a stochastic process with the Gaussian distribution and zero mean value, which is stationary on one or two intervals of duration T. For a single-frequency pulse signal, $R(x,t)$ has the horizontal spatio-temporal coherence form [2, 26–28]

$$\rho_{\text{R}}(x,\tau) \approx J_0\left(\frac{2\pi|x|}{\lambda}\right)\left(1 - \frac{|\tau|}{T}\right)\cos 2\pi f_0\tau, \tag{2}$$

where J_0 is the zeroth-order Bessel function and λ is the wavelength of transmitted signal. The total received signal along the sensor array is written as

$$s_{\text{in}}(x,t) = s_{\text{target}}(x,t) + R(x,t) + n(x,t), \tag{3}$$

where $n(x,t)$ is the environmental noise. In order to extract echoes from environmental noise, the received signal of each sensor is convoluted with $\cos 2\pi f_0 t$

$$\begin{aligned}\bar{s}_{\text{in}}(x,t) &= \frac{2}{G_t T}\int_{t_x}^{T+t_x} s_{\text{in}}(x, t-t')\cos 2\pi f_0 t'\,\mathrm{d}t' \\ &= \bar{s}_{\text{target}}(x,t) + \bar{R}(x,t) + \bar{n}(x,t),\end{aligned} \tag{4}$$

where $t_x = t - x\cos\theta/c$, G_t is the normalization constant and

$$\bar{s}_{\text{target}}(x,t) = \frac{2}{G_t T}\int_{t_x}^{T+t_x} s_{\text{target}}(x, t-t')\cos 2\pi f_0 t'\,\mathrm{d}t', \tag{5}$$

$$\bar{R}(x,t) = \frac{2}{G_t T}\int_{t_x}^{T+t_x} R(x,t-t')\cos 2\pi f_0 t'\,\mathrm{d}t', \tag{6}$$

$$\bar{n}(x,t) = \frac{2}{G_t T}\int_{t_x}^{T+t_x} n(x,t-t')\cos 2\pi f_0 t'\,\mathrm{d}t'. \tag{7}$$

Assuming $M = T/f_0$ is an integer, we can obtain

$$\bar{s}_{\mathrm{target}}(x,t) = \bar{A}\cos 2\pi f_0\left(t + \frac{\cos\theta}{c}x\right), \tag{8}$$

where $\bar{A} = A/G_t$. From equation (6), the power of $\bar{R}(x,t)$ is derived

$$\sigma_{\bar{\mathrm{R}}}^2 = E[\bar{R}(x,t)^2] = \frac{2}{3G_t^2}\sigma_{\mathrm{R}}^2, \tag{9}$$

where σ_{R}^2 is the power of R. For convenience, we can take $G_t = \sqrt{6}\sigma_{\mathrm{R}}/3$, and thus $\sigma_{\bar{\mathrm{R}}}^2$ is normalized to 1. At the same time, the approximate spatio-temporal coherence of $\bar{R}(x,t)$ can be derived:

$$\rho_{\bar{\mathrm{R}}}(x,\tau) \approx J_0\left(\frac{2\pi|x|}{\lambda}\right)\cos 2\pi f_0\tau. \tag{10}$$

Moreover, we can assume that the environmental noise is white and of very small power intensity D_n:

$$E[n(x,t_1)n(x,t_2)] = 2D_n\delta(t_1-t_2), \qquad D_n \to 0. \tag{11}$$

From equation (7), the power of $\bar{n}(x,t)$ is

$$\sigma_{\bar{n}}^2 = E[\bar{n}(x,t)^2] = \frac{4}{G_t^2 T}D_n \to 0, \tag{12}$$

which is quite weak compared with that of the reverberation noise $\bar{R}(x,t)$, and thus $\bar{n}(x,t)$ is neglected hereafter.

From equation (8), the spatial frequency of the target echo in the array direction is $U = f_0\cos\theta/c$. It is well known that realizing SR needs much higher sampling frequencies relative to the input signal. However, the spatial sampling frequencies are limited by the sensor interval l. In order to satisfy the sampling requirement, the signal received by each sensor is delayed by τ_x depending on the sensor position. Based on the fact that

$$s'_{\mathrm{in}}(x,t) = s'_{\mathrm{target}}(x,t) + R'(x,t) = \bar{s}_{\mathrm{in}}(x,t-\tau_x), \tag{13}$$

where $\tau_x = (L\cos\theta - k\lambda)x/Lc$ is the delayed time of the sensor at x, k is a number to be determined, and the facts that

$$s'_{\mathrm{target}}(x,t) = \bar{A}\cos 2\pi\left(f_0 t + \frac{k}{L}x\right), \tag{14}$$

$$R'(x,t) = \bar{R}(x,t-\tau_x), \tag{15}$$

the spatial frequency of the target echo is reduced to $U' = k/L$. From equations (10) and (15), the spatial correlation of $R'(x,t)$ can be derived as

$$C_{\mathrm{R}'}(x) = \langle R'(x_0)R'(x_0+x)\rangle = \sigma_{\bar{\mathrm{R}}}^2 J_0\left(\frac{2\pi|x|}{\lambda}\right)\cos(2\pi f_0\tau_x). \tag{16}$$

3. PSR processing and target detection

Before being sent to the LC detector, the preprocessed signal $s'_{\text{in}}(x, 0)$ is first processed by the bistable system

$$\begin{aligned}\frac{\mathrm{d}y}{\mathrm{d}x} &= ay - by^3 + s'_{\text{in}}(x, 0) \\ &= ay - by^3 + \bar{A}\cos\left(\frac{2\pi k}{L}x\right) + R'(x, 0),\end{aligned} \tag{17}$$

where $a > 0, b > 0$ are the system parameters and y is the system output.

Then the detection problem can be expressed as

$$\begin{cases} H_0 : s'_{\text{in}}(x, 0) = R'(x, 0), \\ H_1 : s'_{\text{in}}(x, 0) = \bar{A}\cos\left(\dfrac{2\pi k}{L}x\right) + R'(x, 0), \end{cases} \tag{18}$$

where H_1 and H_0 are the two hypotheses with and without targets, respectively. We have to decide which hypothesis is correct based on the system output $y(x)$. Let $\mathbf{Y} = [y(x_1), y(x_2), \ldots, y(x_N)]^{\mathrm{T}}$ be the output sample vector and $\mathbf{h} = [h_1, h_2, \ldots, h_N]^{\mathrm{T}}$ be the filter vector. Thus, LC detector based on the output is

$$S(\mathbf{Y}) = \mathbf{h}^{\mathrm{T}}\mathbf{Y}. \tag{19}$$

The performance of such a detector can be evaluated by the deflection which is defined as [29]

$$De(S) = \frac{[E(S|H_1) - E(S|H_0)]^2}{\mathrm{var}(S|H_0)}. \tag{20}$$

The larger the deflection De is, the better the detection performance will be. Denote the output mean-value vectors under H_0 and H_1 as $\mathbf{m}_0$ and $\mathbf{m}_1$, respectively, and the covariance matrix under H_0 as $\mathbf{R}_0$. Thus, for the given $\mathbf{m}_0, \mathbf{m}_1$ and $\mathbf{R}_0$, the maximum deflection value can be obtained when

$$\mathbf{h} = \mathbf{R}_0^{-1}(\mathbf{m}_1 - \mathbf{m}_0), \tag{21}$$

which is the classical matched filter, and the deflection of this detector is

$$De = (\mathbf{m}_1 - \mathbf{m}_0)^{\mathrm{T}}\mathbf{R}_0^{-1}(\mathbf{m}_1 - \mathbf{m}_0). \tag{22}$$

In order to derive $\mathbf{m}_0, \mathbf{m}_1$ and $\mathbf{R}_0$, we need to solve the Fokker–Planck equation (FPE) related to equation (17). However, the exact solutions are very difficult to be obtained, and thus we make some simplifications and approximations as follows.

First, the reverberation noise $R'(x, 0)$ is approximated with the spatial Lorentzian colored noise $\xi(x)$, which has the correlation form

$$C_\xi(x) = \frac{D}{d_x}\exp\left(-\frac{|x|}{d_x}\right), \tag{23}$$

where D is the noise intensity, d_x is the correlation length, which can be determined by

$$D = \sigma^2_{\mathrm{R}'}\big/(4U_{\mathrm{B}}), \tag{24}$$

$$d_x = D\big/\sigma^2_{\mathrm{R}'}, \tag{25}$$

where U_{B} is the bound of the spatial frequency of R'.

Second, the target echo $s'_{\text{target}}(x, 0)$ is approximated with a ladder function $s(x)$

$$s(x) = s_i, \qquad (i-1)\Delta x \leqslant x < i\Delta x, \qquad 1 < i < I, \tag{26}$$

where every period of $s'_{\text{target}}(x, 0)$ is divided into I intervals with length of Δx, and in each interval the target echo is treated as a constant value s_i which is the average in that interval.

Now, in each interval, equation (17) is approximated as

$$\frac{\mathrm{d}y}{\mathrm{d}x} = ay - by^3 + s_i + \xi(x), \qquad 0 < x < \Delta x. \tag{27}$$

The FPE related to system (27) can be derived as [15]

$$\frac{\partial P_i(y,x)}{\partial x} = -\frac{\partial}{\partial y}[c_i(y)P_i(y,x)] + D\frac{\partial^2}{\partial y^2}\left[\frac{1}{1-d_x c_i'(y)}P_i(y,x)\right], \tag{28}$$

where $P_i(y,x)$ is the probability density of the output y in the ith interval, $c_i(y) = ay - by^3 + s_i$, and $c_i'(y)$ is its derivative. The solution of equation (28) can be obtained using the eigenfunction expansion method [22]:

$$P_1(y,x) \approx \sum_{n=0}^{\bar{N}} a_{1n}\Phi_{1n}(y)\exp\left(-\lambda_{1n}\frac{x}{2}\right) + \left[P_1(y,0) - \sum_{n=0}^{\bar{N}} a_{1n}\Phi_{1n}(y)\right]\exp\left(-\lambda_{1(\bar{N}+1)}\frac{x}{2}\right), \tag{29}$$

$$P_i(y,x) \approx \sum_{n=0}^{\bar{N}} a_{\text{in}}\Phi_{\text{in}}(y)\exp\left(-\lambda_{\text{in}}\frac{x}{2}\right) + \left[P_{i-1}(y,\Delta x) - \sum_{n=0}^{\bar{N}} a_{\text{in}}\Phi_{\text{in}}(y)\right]\exp\left(-\lambda_{i(\bar{N}+1)}\frac{x}{2}\right), \tag{30}$$

where λ_{in} is the nth eigenvalue of equation (28) in the ith interval, $\Phi_{\text{in}}(y)$ is the corresponding eigenfunction and $a_{\text{in}}, n = 0, 1, \ldots, \bar{N}$, are constant coefficients. It is assumed that $0 = \lambda_{i0} < \lambda_{i1} \leqslant \cdots \leqslant \lambda_{i(\bar{N}+1)}$ and λ_{i1} is called the system response speed in the ith interval [16]. Thus, with the given initial probability density function $P_1(y,0)$, $P_i(y,x)$ can be calculated from equation (30) recursively and then the mean-value vector $\mathbf{m}_1$ will be obtained.

Under the H_0 hypothesis, s_i will become zero in equation (27). When the system reaches its stable status, the system output will have zero mean value all the time, and thus $\mathbf{m}_0 = 0$. In addition, the transition probability density $P_0(y, x|y', 0)$ under H_0 also obeys the same FPE

$$\frac{\partial P_0(y,x|y',0)}{\partial x} = -\frac{\partial}{\partial y}[c_0(y)P_0(y,x|y',0)] + D\frac{\partial^2}{\partial y^2}\left[\frac{1}{1-d_x c_0'(y)}P_0(y,x|y',0)\right], \tag{31}$$

where $c_0(y) = ay - by^3$ and $c_0'(y)$ is its derivative. Its solution also can be expanded as

$$P_0(y,x|y',0) \approx \sum_{n=0}^{\bar{N}} a_{0n}(y')\Phi_{0n}(y)\exp\left(-\lambda_{0n}\frac{x}{2}\right) + \left[\delta(y-y') - \sum_{n=0}^{\bar{N}} a_{0n}(y')\Phi_{0n}(y)\right]\exp\left(-\lambda_{0(\bar{N}+1)}\frac{x}{2}\right). \tag{32}$$

Then we obtain the auto-correlation function of the output y under H_0

$$r_y(x) = \iint yy' P_0(y,x|y',0)P_0(y')\,\mathrm{d}y\,\mathrm{d}y', \tag{33}$$

where $P_0(y')$ is the stable probability density function of the output under H_0. Based on these, the covariance matrix $\mathbf{R}_0$ can be derived, and also the deflection measure $De = \mathbf{m}_1^{\mathrm{T}}\mathbf{R}_0^{-1}\mathbf{m}_1$ can be calculated.

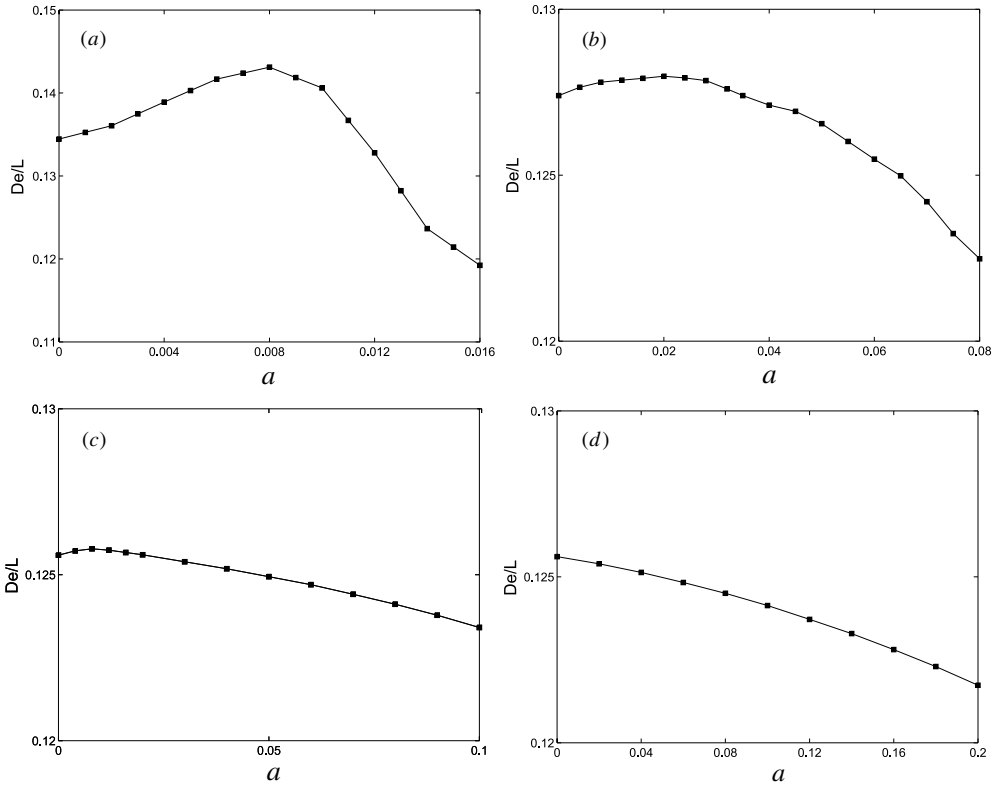

Figure 3. The relationships between the system efficiency De/L and parameter a for different values of U', with $D = 0.0167$, $d_x = 0.0167$, $\bar{A} = 0.1$ and $I = 6$. (*a*) $U' = 1/72$, $\bar{b} = 0.0046$; (*b*) $U' = 1/36$, $\bar{b} = 0.085$; (*c*) $U' = 1/18$, $\bar{b} = 0.59$; (*d*) $U' = 1/9$, $\bar{b} = 2.97$.

The values of $\mathbf{m}_0$, $\mathbf{m}_1$ and $\mathbf{R}_0$ will change with the values of system parameters a and b, which, in turn, cause the change of the deflection measure De. Therefore, the system parameters a and b must be tuned properly to maximize De. For every pair values of a and b, the calculation of De needs to solve the corresponding FPEs. In [16], the parameters are tuned to maximize the performance measure under the condition that the system response speed is constant. Our research reveals that the maximizer a^* is always very close to zero, and a small change of a value will not cause the change of the system response speed. Based on these facts, we propose a simplified algorithm to search for the values of the system parameters a and b to maximize the detection performance. In this algorithm, we first let a be zero, and then the system parameter b is tuned to the value $\bar{b}$ to satisfy the condition that the average system response speed $\bar{\lambda}_1(0, \bar{b}) = \frac{1}{I}\sum_{i=1}^{I} \lambda_{i1}(0, \bar{b}) = 3U'$. After this, we tune the system parameter a to maximize De under the condition of $b = \bar{b}$. The related optimization problem can be constructed as follows:

$$\max_{a\rangle 0, \bar{\lambda}_1(0,b)=3U'} De. \tag{34}$$

In figure 3, the relationships between the system efficiency De/L and the parameter a are shown for different values of U'. From this figure, we can note that the system efficiency can be maximized by tuning the parameter a properly for signals with slow frequencies. However,

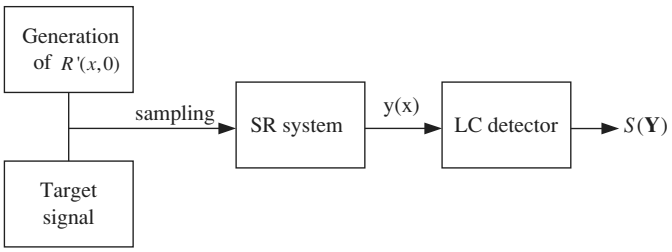

Figure 4. The block scheme for simulating system.

the system efficiency will decrease monotonically with the parameter a, if the value of U' exceeds a certain value. In this case, we can just let a be zero.

Now we assume the length of input signals is large enough. According to the central limit theorem, the output $S(\mathbf{Y})$ of the LC detector can be treated as a Gaussian stochastic variable with zero mean and the variance of $\mathrm{var}(S|H_0) = \mathbf{h}^{\mathrm{T}}\mathbf{R}_0\mathbf{h} = De$ under H_0 hypothesis. It is a Gaussian random variable with the mean of $E(S|H_1) = \mathbf{h}^{\mathrm{T}}\mathbf{m}_1 = De$ under H_1 hypothesis. The variance of $S(\mathbf{Y})$ under H_1 hypothesis also can be derived based on the solution to the related FPEs. Our research further reveals that, under the condition of weak SRR, the variances of $S(\mathbf{Y})$ under both H_1 and H_0 are almost the same. For simplicity, we can take $\mathrm{var}(S|H_1) \approx \mathrm{var}(S|H_0) = De$ in this paper. Now, the decision can be made as follows:

$$S(\mathbf{Y}) \underset{H_0}{\overset{H_1}{\gtrless}} \eta, \tag{35}$$

where η is the threshold which is determined according to the desired probability of false alarm.

4. Numerical simulation and results

In order to verify the efficiency of our proposed detection system, numerical simulations are performed. The simulation system is shown in figure 4. For simplicity, we assume that the signals have been preprocessed, and thus our simulations start from equation (17). In order to generate the reverberation noise, a white Gaussian noise is filtered by a designed filter so that the correlation required by equation (16) can be satisfied. The generated noise is then added to the target signal to form the noisy signal which will be sampled and sent to the SR system. Finally, the output of the SR system is received and processed by the LC detector to make decisions.

In our simulations, we assume that the active sonar emits a pulse with frequency $f_0 = 15$ kHz and duration $T = 1$ ms, and thus $M = T/f_0 = 15$. A target echo arrives at the sensor array with angle $\theta = 60^\circ$. The interval between two adjacent sensors is $l = 0.05$ m. In addition, we assume that the SRR of received signal is weak and has the value of $A^2/2\sigma_R^2 = 1/300$, and thus $\bar{A} = TA/2G_t = \sqrt{6}A/2\sigma_R = 0.1$.

First, we assume the sensor array is of enough length. The relationships between the maximum efficiency De/L and the reduced spatial frequency $U' = k/L$ are shown in figure 5. The line marked with '○' is obtained based on the theoretical analysis. Here we divide each period of target signals into $I = 6$ intervals, and the target signals are considered to be constant in each interval. The line marked with '△' is obtained by the Monte Carlo simulations. It is

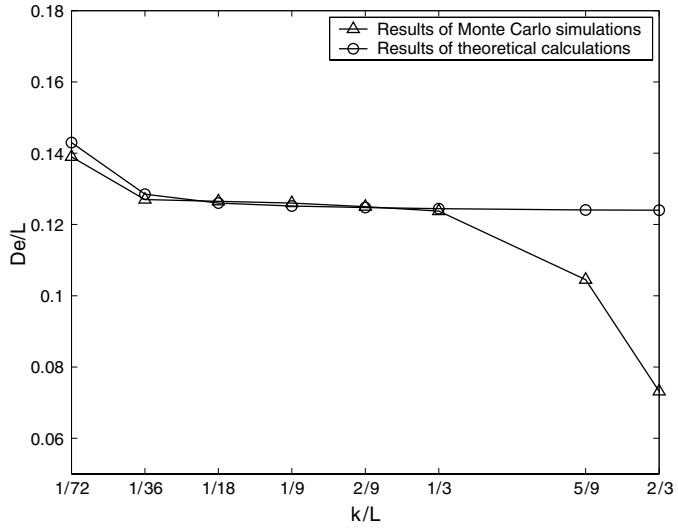

Figure 5. The relationships between the maximum efficiency De/L of the detection system in figure 4 and reduced spatial frequency $U' = k/L$ of the target signal.

noticed that the efficiencies obtained from theoretical analysis and simulations both decrease with increasing U'. However, when U' becomes higher, the simulation results will decrease faster than the theoretical results. The reason is that the theoretical results are based on the continuous system described by equation (17), while the simulation results are based on the signals sampled by the sensors at the rate of $U_s = 1/l$. When U' becomes larger enough, the spatial sampling frequency U_s will not satisfy the sampling requirement any more. This is also the reason why the spatial frequencies of target echoes have to be reduced before being processed.

Then, we assume that the sensor array is of the limited length $L = 9$ m. In order to construct input signals with longer length, we propose an unfolding method. By letting

Case 1. $k = 1, 2, 3, \ldots,$

$$s''_{\text{in}}(x) = s'_{\text{in}}\left(x - nL, \frac{n}{f_0}\right) = \bar{A}\cos\left(\frac{2\pi k}{L}x\right) + R'\left(x - nL, \frac{n}{f_0}\right),$$
$$0 \leqslant x \leqslant L' = ML, \tag{36}$$

Case 2. $k = \frac{1}{2}, \frac{1}{4}, \frac{1}{8}, \ldots,$

$$s''_{\text{in}}(x) = s'_{\text{in}}\left(x - nL, \frac{nk}{f_0}\right) = \bar{A}\cos\left(\frac{2\pi k}{L}x\right) + R'\left(x - nL, \frac{nk}{f_0}\right),$$
$$0 \leqslant x \leqslant L' = \frac{ML}{k}, \tag{37}$$

where $n = \lfloor x/L \rfloor$ is the floor number of x/L, the spacetime signal $s'_{\text{in}}(x, t)$ is unfolded to a one-dimensional spatial signal $s''_{\text{in}}(x)$ with the length of L'. Thus, the simulation system is modified as shown in figure 6, where an unfolding block is inserted between the signal generation block and the SR system.

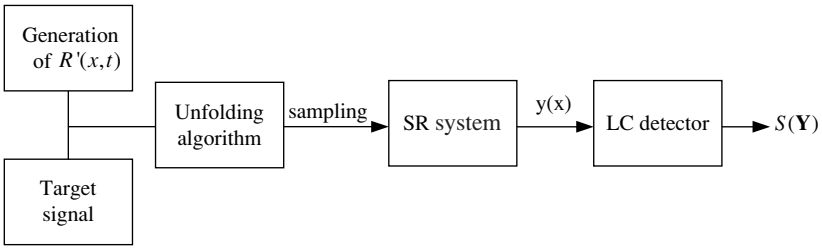

Figure 6. The modified block scheme for simulating system.

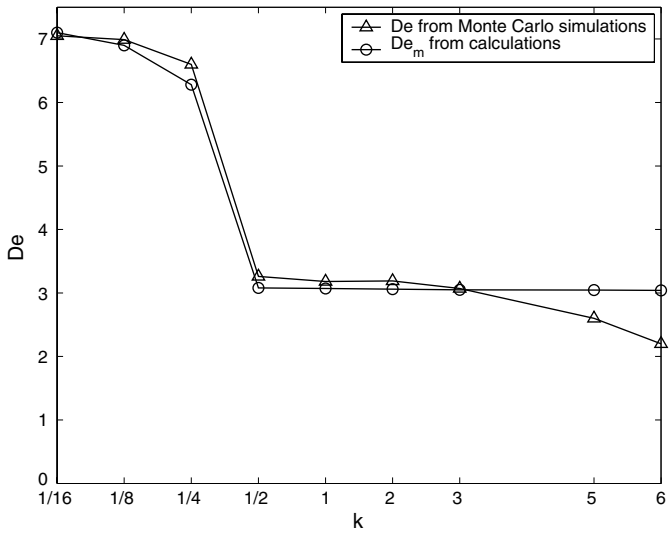

Figure 7. The relationships between the maximum deflection De of the detection system in figure 6 and the parameter k.

The original theoretical results are obtained by treating $R'(x - nL, n/f_0)$, or $R'(x - nL, nk/f_0)$ in case 2, in the same way as $R'(x, 0)$. According to equation (10), the correlation of $R'(x - nL, n/f_0)$, or $R'(x - nL, nk/f_0)$ in case 2, is varied with n. After adopting the unfolding method, the original theoretical results should also be modified. It is obvious that the mean values of $S(\mathbf{Y})$ under both H_0 and H_1 will stay the same, and thus we only need to change its variances to $\mathrm{var}_\mathrm{m}(S|H_0) \approx \mathrm{var}_\mathrm{m}(S|H_1) = \alpha_k De$, where α_k is called the modified coefficient. Hence, the deflection measure $De_\mathrm{m} = De/\alpha_k$. The value of α_k can be determined from simulations. For case 1 and $k = 1/2$, we can get $\alpha_k \approx 0.37L'/L$. For other cases, we can get $\alpha_k \approx 0.18L'/L$.

Figure 7 shows the relationships between the deflection measure and k. We can note that the smaller the value of k is, the larger the deflection measure will be. If $k > 1$, there is almost no change in the modified deflection De_m. However, when $k > 3$, the simulation results will deviate from the theoretical results, because of the unsatisfied sampling requirement.

According to the binary test of equation (35), the probability of false alarm (H_1 is accepted when, in fact, H_0 is true) and the probability of detection (H_1 is accepted when, in fact, H_1 is

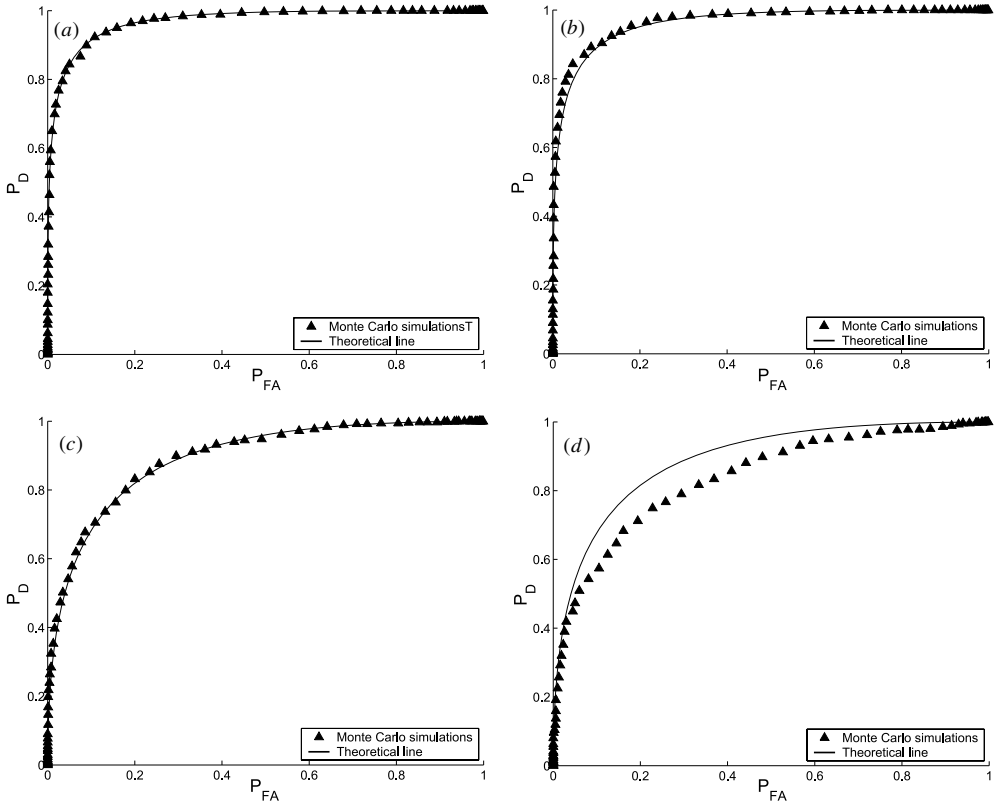

Figure 8. ROC curves of the detection system in figure 6 for different values of k. ROC curves for (*a*) $k = 1/8$, (*b*) $k = 1/4$, (*c*) $k = 1$ and (*d*) $k = 6$.

true) can be expressed as

$$P_{\mathrm{FA}} = \int_{\eta}^{\infty} P_S(x|H_0)\,\mathrm{d}x, \tag{38}$$

$$P_{\mathrm{D}} = \int_{\eta}^{\infty} P_S(x|H_1)\,\mathrm{d}x, \tag{39}$$

where $P_S(x|H_0)$ and $P_S(x|H_1)$ are the probability density functions of the statistic $S(\mathbf{Y})$ under H_0 and H_1 hypotheses, respectively. As stated previously in the last paragraph of section 3, $S(\mathbf{Y})$ can be treated as Gaussian distributed with the same variance under both hypotheses. Namely, there are

$$S(\mathbf{Y}|H_0) \sim N(0, \alpha_k De), \qquad S(\mathbf{Y}|H_1) \sim N(De, \alpha_k De), \tag{40}$$

where $N(m, \sigma^2)$ refers to the Gaussian distribution with mean m and variance σ^2. Thus, equations (38) and (39) become

$$P_{\mathrm{FA}} \approx \frac{1}{2}\mathrm{erfc}\left(\frac{\eta}{\sqrt{2\alpha_k De}}\right), \tag{41}$$

$$P_{\mathrm{D}} \approx \frac{1}{2}\mathrm{erfc}\left(\frac{\eta - De}{\sqrt{2\alpha_k De}}\right), \tag{42}$$

where $\mathrm{erfc}(x) = 2/\sqrt{\pi}\int_x^\infty \exp(-t^2)\,\mathrm{d}t$ is the complementary error function. Both P_D and P_FA are functions of the threshold η. The plot of P_D versus P_FA is called the receiver operating characteristic (ROC) curve that describes the performance of the hypothesis test. Figure 8 demonstrates performances of our proposed detection system with ROC curves. In this figure, the theoretical lines are derived from equations (41) and (42), and for the cases of $k = 1/8$, $k = 1/4$ and $k = 1$, the ROC curves derived by the Monte Carlo simulations match the theoretical results quite well. From this figure, we can also find that the smaller the value of k is, the better the detection performance will be. However, when $k < 1/4$, the improvement of detection performance is quite limited, and according to case 2 described by equation (37), a smaller k will induce a larger L', and in turn, will increase the computational load.

5. Conclusion

In this paper, parameter-induced stochastic resonance techniques are applied to the target detection in the presence of shallow-water reverberation. For this purpose, the input signals are preprocessed to form the inputs to the bistable SR system. In addition, the unfolding method is suggested to construct signals with longer length for the sensor array with limited length. Based on the solutions to the related FPEs, the performance of our proposed detection system can be derived in terms of the deflection measure. The detection performance is affected by the choice of the parameter values of the bistable stochastic resonance system, and thus will be maximized by tuning system parameters properly based on PSR techniques. The theoretical analysis and the efficiency of our proposed detection system are verified by numerical simulations. Our research proposes a peculiar way to detect targets in the presence of shallow-water reverberation. Our future work will focus on the target detection under more complicated situations, such as directive sources, narrow band signals and non-Gaussian reverberations.

Acknowledgments

The authors greatly appreciate the support provided by the National Natural Science Foundation of China (no 10772161) and the National Natural Science Foundation for the Youth of China (no 60702022).

References

[1] Etter P C 2003 *Underwater Acoustic Modeling and Simulation* 3rd edn (London: Spon)
[2] Olshevskii V V 1967 *Characteristics of Sea Reverberation* (New York: Consultants Bureau)
[3] Olshevskii V V 1978 *Statistical Methods in Sonar* (New York: Consultants Bureau)
[4] Alexandrou D, Demoustier C and Haralabus G 1992 *J. Acoust. Soc. Am.* **91** 1403–13
[5] Benzi R, Sutera A and Vulpiani A 1981 *J. Phys. A: Math. Gen.* **14** 453–7
[6] Nicolis C and Nicolis G 1981 *Tellus* **33** 225–34
[7] Gammaitoni L, Hanggi P, Jung P and Marchesoni F 1998 *Rev. Mod. Phys.* **70** 223–87
[8] Collins J J, Chow C C and Imhoff T T 1995 *Nature* **376** 236–8
[9] Kiss L 1996 *Chaotic, Fractal, and Nonlinear Signal Processing* (*AIP Conf. Proc.* vol 375) ed R Katz pp 382–96
[10] Loerincz K, Gingl Z and Kiss L 1996 *Phys. Lett.* A **224** 63–7
[11] Chapeau-Blondeau F 1999 *Int. J. Bifurcation Chaos* **9** 267–72
[12] Gingl Z, Makra P and Vajtai R 2001 *Fluctuation Noise Lett.* **1** L181–8
[13] Zozor S and Amblard P O 2002 *Signal Process.* **7** 353–67
[14] Xu B, Duan F, Bao R and Li J 2002 *Chaos Solitons Fractals* **13** 633–44
[15] Xu B, Li J, Duan F and Zheng J 2003 *Chaos Solitons Fractals* **16** 93–106
[16] Xu B, Li J and Zheng J 2003 *J. Phys. A: Math. Gen.* **36** 11969–80

[17] Xu B, Duan F and Chapeau-Blondeau F 2004 *Phys. Rev.* E **69** 061110
[18] Asdi A and Tewfik A 1995 *Proc. Int. Conf. Acoust., Speech, Signal Process. (ICASSP 95)* vol 2 pp 1332–5
[19] Kay S 2000 *IEEE Signal Process. Lett.* **7** 8–10
[20] Chen H, Varshney P, Kay S and Michels J H 2006 *Proc. 40th Ann. Conf. Inf. Sci. Syst.* pp 56–61
[21] Duan F and Xu B 2003 *Int. J. Bifurcation Chaos* **13** 411–25
[22] Li J and Xu B 2006 *Int. J. Bifurcation Chaos* **16** 427–35
[23] Duan F and Abbott D 2007 *Physica* A **376** 173–90
[24] Rousseau D, Rojas-Verela J, Duan F and Chapeau-Blondeau F 2005 *Int. J. Bifurcation Chaos* **15** 667–79
[25] Duan F, Abbott D and Gao Q 2005 *Fluctuation Noise Lett.* **5** L127–42
[26] Cron B F and Sherman C H 1962 *J. Acoust. Soc. Am.* **34** 1732–6
[27] Urick R J and Lund G R 1970 *J. Acoust. Soc. Am.* **47** 109–11
[28] Jackson D R and Moravan K Y 1984 *J. Acoust. Soc. Am.* **75** 428–36
[29] Picinbono B 1995 *IEEE Trans. Aerosp. Electron. Syst.* **31** 1072–81